International Journal of Thermophysics, Vol. 19, No. 4, 1998

Cancellation of the Heating Piston Effect by Convective Enhancement of a Cooling Piston Effect[1]

A. Jounet,[2,3] S. Amiroudine,[4] A. Mojtabi,[2] and B. Zappoli[4]

This work brings new insight to the question of the piston effect, which has been found to be the main cause of temperature equilibration in the vicinity of the liquid–vapor critical point under weightlessness conditions. The thermalization process of a near-critical fluid confined in a cavity and submitted to local heating is modeled with special emphasis on the role of gravity and boundary conditions. The solution of the unsteady Navier–Stokes equations written for a hypercompressible low-heat-diffusing van der Waals gas is obtained in a 2-D configuration by means of a finite-volume numerical code. Under Earth gravity conditions, the results show that the thermal plume rising from a heat source strongly decreases and rapidly cancels bulk fluid heating when it strikes the top thermostated wall. It is proved that convection does not prevent heat transfer by the piston effect but that it causes a sudden enhancement of the cooling piston effect generated at the thermostated top boundary, which leads to an early equilibrium between the cooling and heating piston effects.

KEY WORDS: acoustic waves; convection; diffusion; heat transfer; near-critical fluid; piston effect.

1. INTRODUCTION

It has recently been found that the fast temperature equilibration occurring in near-critical fluids under conditions of weightlessness is achieved by a new process called the piston effect (PE). In fact, when a confined near-critical fluid is heated at its boundaries, the fluid contained in the thin

[1] Paper presented at the Thirteenth Symposium on Thermophysical Properties, June 22–27, 1997, Boulder, Colorado, U.S.A.

[2] Institut de Mécanique des Fluides de Toulouse, UMR CNRS/INP-UPS 5502, UFR MIG, Université Paul Sabatier, 118, Route de Narbonne, 31062 Toulouse Cédex, France.

[3] To whom correspondence should be addressed.

[4] Centre National d'Etudes Spatiales, 18, Av. E. Belin, 31405 Toulouse Cédex 04, France.

0195-928X/98/0700-1185$15.00/0

thermal adaptation layer expands strongly because of its diverging compressibility. This expansion adiabatically compresses the rest of the fluid and causes a homogeneous increase in the temperature. In contrast with pure diffusion, this thermoacoustic mechanism becomes increasingly efficient as the critical point is approached, and the thermal equilibration time becomes shorter. First theoretically predicted by different teams in 1990 [1–3], the PE has been extensively explored in several analytical [4–6], numerical [7, 8], and experimental [9, 10] studies.

Despite the high hydrodynamic instability observed on the ground in near-critical fluids, it has been recently shown that the PE is still present under $1g$ conditions [8]. Indeed, even if the temperature is almost homogeneous in the whole fluid due to the PE, a very small temperature inhomogeneity causes a large density inhomogeneity in such a hypercompressible fluid. Thus, the steep density gradients that appear in the thermal boundary layer trigger a strong flow in a quasi-isothermal fluid. Nevertheless, recent experiments performed on Earth [11] have shown that the near-critical fluid heated by a local heat source in a noninsulated cell undergoes almost no warming compared with that observed under microgravity conditions. In the present study, we reproduced similar conditions in our simulation code to understand the physical processes which caused this result. The influences of the thermal boundary conditions and of convection are clearly established. In particular, it is shown that when the hot convective plume rising from the thermistor strikes the thermostated upper wall, the cooling PE generated at this boundary is strongly enhanced, thus drastically slowing down the homogeneous heating of the bulk phase. Then, the cooling and heating PE quickly balance each other as the cold boundary layer (CBL) becomes entirely covered by the flow, and the bulk fluid temperature stops increasing.

The model and the governing equations are presented in Section 2, and the numerical method in Section 3, while Section 4 is dedicated to the results and discussion.

2. THE MODEL AND GOVERNING EQUATIONS

The model used to simulate the behavior of the supercritical fluid is the same as the one already used in Refs. 4, 5, and 8. We consider a 2-D square cavity filled with near-critical CO_2 submitted to gravity. The heat source, located at the center of the domain, provides constant power, while all the boundaries are adiabatic, except the top wall, which is maintained at a constant temperature (Fig. 1). The fluid is initially at rest, stratified in density and at thermal equilibrium.

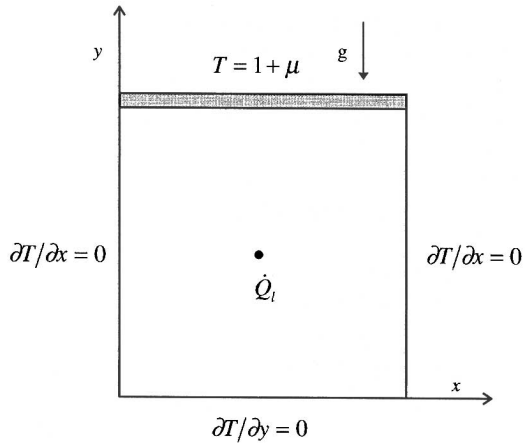

Fig. 1. The center-heated 2-D square cavity.

The nondimensional variables (density, temperature, pressure, velocity, space, and time) introduced in the conservation equations are defined as

$$\rho = \frac{\rho'}{\rho'_c}; \qquad T = \frac{T'}{T'_c}; \qquad P = \frac{P'}{\rho'_c R' T'_c}; \qquad \vec{v} = \frac{\vec{v}'}{c'_0}; \qquad \vec{x} = \frac{\vec{x}'}{L'}; \qquad t = \frac{t'}{t'_a}$$

where ρ'_c and T'_c are the critical coordinates (467.8 $kg \cdot m^{-3}$ and 304.13 K, respectively), R' is the gas constant, $c'_0 = \sqrt{\gamma_0 R' T'_c}$ the sound velocity for the perfect gas in which γ_0 is the specific heat ratio (for the perfect gas), L' the length of the cavity (10 mm), and $t'_a = L'/c'_0$ a characteristic acoustic time.

The thermistor is simulated by means of local power injection inserted in the energy equation by the nondimensional term: r. $r = r'/r'_0$, with $r'_0 = \rho'_c R' T'_c c'_0 / L'(\gamma_0 - 1)$ and $r' = \dot{Q}'_l / S'_Q$, where $\dot{Q}'_l$ represents the heating rate per unit length (0.74 $W \cdot m^{-1}$ in our case) and S'_Q the section of the wire representing the thermistor.

Concerning the model of the critical behavior, besides the van der Waals equation of state, which exhibits a $(T' - T'_c)^{-1}$ divergence of compressibility, the following law is used to take the thermal conductivity divergence into account: $\lambda = \lambda'/\lambda'_0 = 1 + 0.75((T' - T'_c)/T'_c)^{-1/2}$. Both these equations were chosen with a concern for simplicity. Even though they do not lead to the correct critical exponents, they permit rich phenomenological investigations, which have already provided some very relevant qualitative information on the processes occurring in near-critical fluids. More information concerning this choice can be found in previous studies [4–6, 8].

Then the resulting system of equations is

$$\frac{\partial \rho}{\partial t} + \nabla \cdot (\rho \vec{v}) = 0 \tag{1}$$

$$\frac{\partial (\rho \vec{v})}{\partial t} + \nabla \cdot (\rho \vec{v} \otimes \vec{v}) = -\gamma_0^{-1} \nabla P + \varepsilon \left[\nabla^2 \vec{v} + \frac{1}{3} \nabla (\nabla \cdot \vec{v}) \right] + \frac{1}{Fr_0} \rho \vec{g} \tag{2}$$

$$\begin{aligned} \frac{\partial (\rho T)}{\partial t} + \nabla \cdot (\rho \vec{v} T) = & -(\gamma_0 - 1) \left(P + \frac{9}{8} \rho^2 \right) (\nabla \cdot \vec{v}) \\ & + \frac{\varepsilon \gamma_0}{\mathrm{Pr}_0} \nabla \cdot [(1 + 0.75(T-1)^{-0.5}) \nabla T] \\ & + \varepsilon \gamma_0 (\gamma_0 - 1) \left(v_{i,j} v_{j,i} + v_{i,j} v_{i,j} - \frac{2}{3} v_{i,i} v_{j,j} \right) + r \end{aligned} \tag{3}$$

$$P = \frac{\rho T}{1 - (1/3)\rho} - \frac{9}{8} \rho^2 \tag{4}$$

where $\mathrm{Pr}_0 = \nu_0'/\chi_0'$ represents the Prandtl number (ν_0' and χ_0' are the reference kinematic viscosity and thermal diffusivity, respectively, at the critical density for an ideal gas), $Fr_0 = c_0'^2/L' g_0'$ is the Froude number with $g_0' = 9.8\ \mathrm{m \cdot s^{-2}}$, and $\varepsilon = \mathrm{Pr}_0\, t_a'/t_d'$ ($t_d' = L'^2/\chi_0'$).

In the vicinity of the critical point, the initial conditions can be written as

$$\vec{v} = 0; \qquad T = 1 + \mu; \qquad \rho(y) = \exp(-K(y-1));$$

$$P(y) = \tfrac{3}{2}(1+\mu) - \tfrac{9}{8} + \tfrac{9}{4}\mu \exp(-K(y-1))$$

with $\mu = (T_i' - T_c')/T_c'$ (T_i' the initial temperature, taken 1 K warmer than T_c' in our calculations) and $K = 4g\gamma_0/9\mu Fr_0$ (g is the nondimensional gravity level).

At the boundaries, the conditions are $\vec{v} = 0$, $T(y=1) = 1 + \mu$, and $\partial T/\partial n (y \neq 1) = 0$.

In this study, we are not interested in the description of acoustic waves, and since the flow Mach number is very low, the pressure is split into two parts and the equations are rescaled with a longer reference time (acoustic filtering method; see Ref. 12). Thus, one chooses the PE time scale [4, 5], which is smaller than the convection time scale: $\tau = t\varepsilon/\mu^{3/2}$, while the corresponding reference velocity is given by $U' = c_0' \varepsilon/\mu^{3/2}$.

3. NUMERICAL METHOD

The numerical method adopted in our code is the finite-volume method using a staggered grid in order to avoid pressure oscillations [13]. The SIMPLER algorithm [13] was used to perform the resolution. At the discretization stage, a power-law scheme was used in the model. Because of the question of the influence that the artificial viscosity might have on the results [14], the calculations were also tested with a QUICK scheme [15], without great changes being exhibited.

The mesh frame was refined in the thermal boundary layer regions, i.e., at the center of the cell and close to the top wall, by means of a power-law series. But since the flow was found to be rather turbulent in the presence of gravity, the grid must also be thin over the whole domain. Such constraints led us to choose a 200×200-point mesh with a 1.6 boundary refining exponent and a resulting time step of 5×10^{-3}.

4. RESULTS AND DISCUSSION

4.1. Flow Pattern

Because of the large compressibility and very low diffusivity of the fluid, steep density gradients (about $5 \times 10^4\ \mathrm{kg \cdot m^{-4}}$) appear close to the heat source, which is only 2 K warmer than the initial temperature. Consequently, the buoyancy force generates an intense flow (velocity reaches 15 $\mathrm{mm \cdot s^{-1}}$) which looks like a plume rising to the top wall (Figs. 2–5). The temperature of the convected fluid rapidly decreases as it rises. Only the small portion of fluid located in the core of the plume is significantly warmer than the rest of the fluid, and neither convection nor diffusion carries away a lot of heat. Thus, the PE remains the main cause of the bulk temperature increase. A cooling PE (CPE) appears because of the thermostated wall: a very thin thermal adaptative layer (the CBL) forms in which the hypercompressible fluid strongly contracts due to the cooling imposed by the wall, and in turn it generates the expansion acoustic waves causing homogeneous cooling of the fluid. Therefore, the PE results from the competition between the heating PE (HPE), produced by the fluid heated by the thermistor, and the CPE.

After less than 1 s, the upward plume strikes the top wall and is spread along it in a quasi-turbulent way. Indeed, in addition to both rotative cells formed by viscous coupling, the cooler fluid located in the CBL tends to flow down, like dripping liquid, while the fluid convected in the plume is still buoyant. Some recirculation flows appear on either side of the stagnation point area, and the CBL structure is greatly modified. Two essential

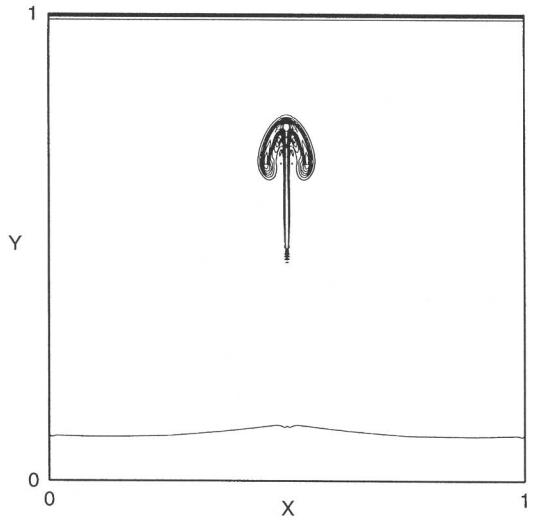

Fig. 2. Thermal field at $\tau = 2$.

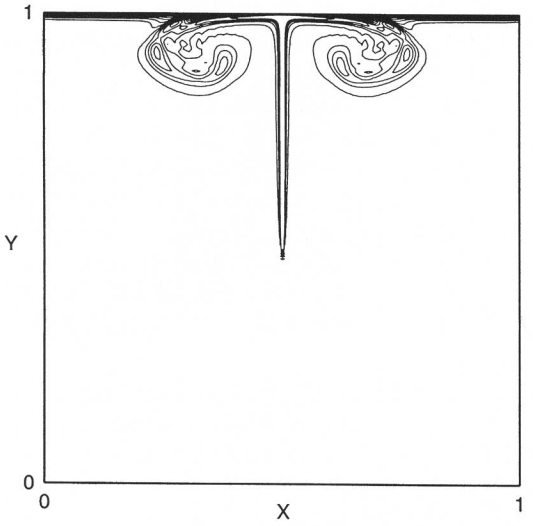

Fig. 3. Thermal field at $\tau = 5$.

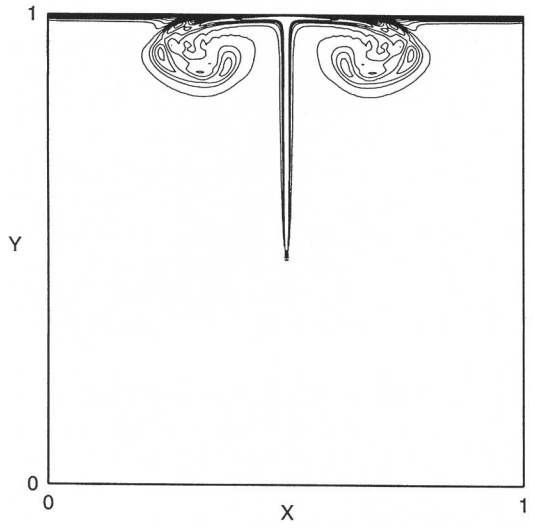

Fig. 4. Thermal field at $\tau = 10$.

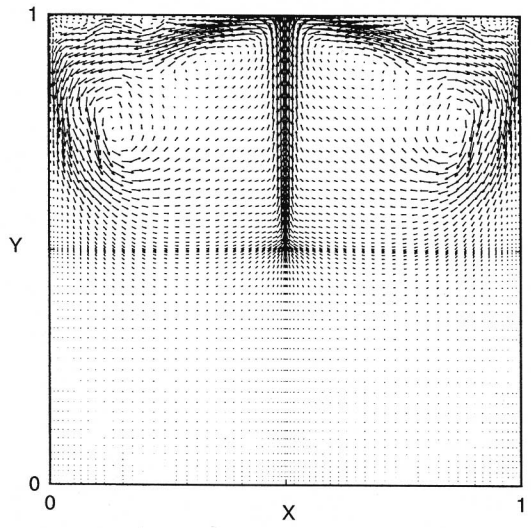

Fig. 5. Velocity field at $\tau = 10$.

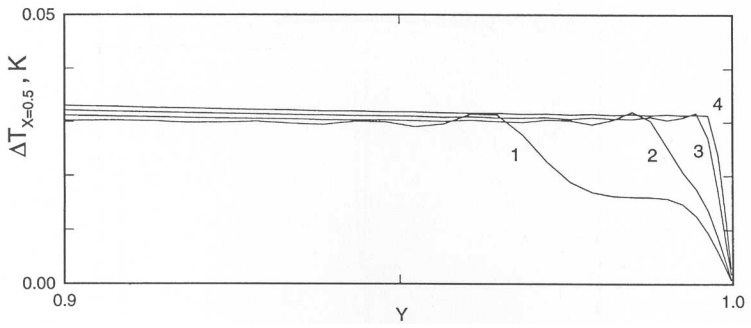

Fig. 6. Temperature elevation profiles close to the CBL at the time of the first shock of the plume: $\tau = 3.2$ (curve 1), $\tau = 3.4$ (2), $\tau = 3.6$ (3), and $\tau = 3.8$ (4).

steps occur during the CBL structural changes, and their effects on cavity thermalization are discussed in the next section. First, around $\tau = 3.5$ (0.8 s), the rising flow begins to strike the middle of the top wall. The temperature elevation profile at this moment is plotted in Fig. 6. It can be observed that the gradients suddenly increase in the CBL due to convection which reduces the diffusion layer thickness and, at the same time, makes the outer temperature of the CBL warmer. Second, at $\tau = 9$, sudden temperature gradient increases occur on both corners of the CBL (Fig. 7): a warmer quasi-bubble becomes separated from the vortex flows because of the buoyancy and strikes both sides of the isothermal wall.

4.2. Fluid Thermalization

The temperature variations caused by the PE, measured at a point of the cavity where neither convection nor diffusion brings any heat, are plotted versus time in Fig. 8. After a continuous increase, two changes of slope appear around $\tau = 3.5$ and $\tau = 9$ (2.1 s), followed by an almost-constant value (28 mK). This early end to heating by the PE contrasts with what

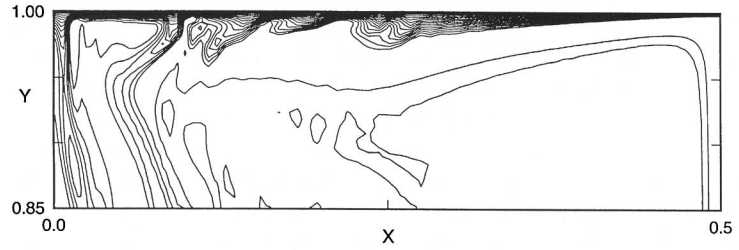

Fig. 7. Thermal field close to the CBL at $\tau = 9.2$.

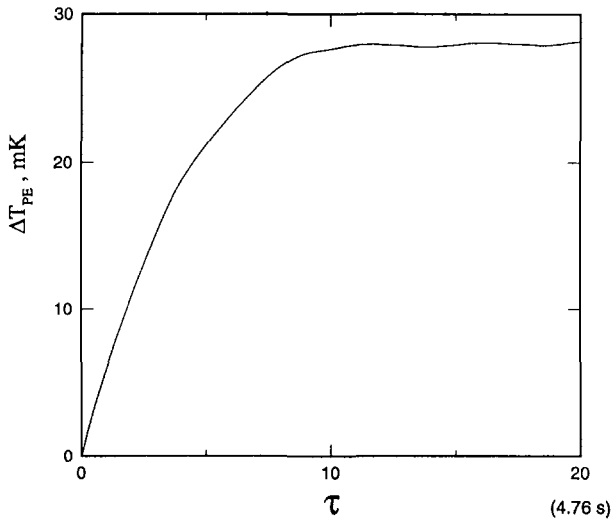

Fig. 8. Temperature variations in the bulk fluid versus time.

happens at $g = 0$, the temperature elevation of which is plotted in Fig. 9, curve 2 (curve 1 represents the plot of Fig. 8), and which exhibits a continuous increase. In curves 3 and 4 in Fig. 9 all the walls are insulated in the presence (3) or absence (4) of gravity. They show that the HPE is only slightly disturbed by convection, as already observed in another configuration [8], and they prove that the end to heating observed in Fig. 8 is necessarily due to the CPE. These curves also show that the (constant) fluid heating rate by the PE is proportional to the injected heat flux, a result which is consistent with previous analytical works [5, 6]. Similarly, the changes of slope appearing in Fig. 8 occur at the same times as those of the total heat flux lost at the thermostated wall, and the heating by PE stops when this heat flux equals the power injected by the thermistor (Fig. 10). The local thermal gradient increases in the CBL, pointed out in the previous section at $\tau = 3.5$ and $\tau = 9$, correspond to sudden enhancements of thermal diffusion driven by convection. In turn, these local enhancements of the fluid cooling in the CBL generate stronger CPEs. Therefore, the changes in fluid heating rate correspond to local and sudden CPE enhancements. From $\tau = 10$ (2.38 s), the CPE gets strong enough to balance the HPE. Then since no major changes affect the CBL thermal structure despite the very transient nature of the flow, bulk heating by the PE stops. The almost-total absence of heating over long periods observed experimentally in a near-critical fluid thus seems to result from the cancellation of the two conflicting PEs, which is accelerated by convection near the CBL.

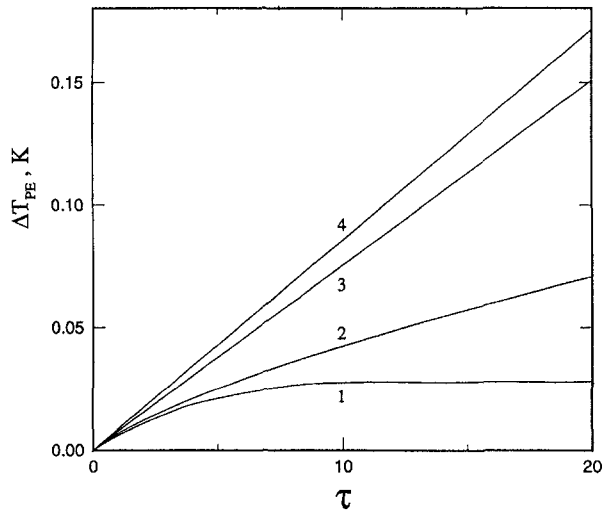

Fig. 9. Comparison of the PE heating for $g = 1$ (curves 1 and 3) or $g = 0$ (curves 2 and 4), with the upper wall being either thermostated (curves 1 and 2) or adiabatic (curves 3 and 4).

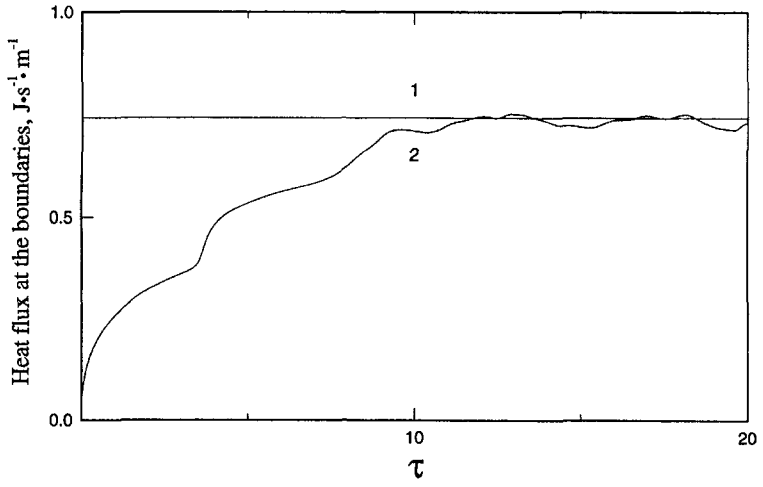

Fig. 10. Heat fluxes injected by the thermistor (curve 1) and lost at the non-insulated boundary (curve 2) versus time.

5. CONCLUSION

The mechanism of temperature equilibration in a locally heated near-critical pure fluid under Earth gravity conditions has been identified by means of numerical simulations. Some new insights into the question of the interplay between convection and the piston effect have been gained. In particular, it has been found that, far from being due to the cancellation of the piston effect by convection, the absence of piston effect heating results from an enhancement of the cooling piston effect which occurs when the temperature field is locally modified by convection close to the thermostated boundary. A balance between the heating piston effect and the cooling piston effect can then soon appear, which stops any overall piston effect heating.

REFERENCES

1. B. Zappoli, D. Bailly, Y. Garrabos, B. Le Neindre, P. Guenoun, and D. Beysens, *Phys. Rev. A* **41**:2264 (1990).
2. H. Boukari, J. N. Shaumeyer, M. E. Briggs, and R. W. Gammon, *Phys. Rev. A* **41**:2260 (1990).
3. A. Onuki, H. Hao, and R. A. Ferrel, *Phys. Rev. A* **41**:2256 (1990).
4. B. Zappoli, *Phys. Fluids A* **4**:1040 (1992).
5. B. Zappoli and P. Carlès, *Eur. J. Mech. B* **14**:1 (1995).
6. P. Carlès, *Etude de l'Effet Piston et des Phénomènes Thermoacoustiques dans les Fluides Supercritiques*, Ph.D. dissertation (Institut National Polytechnique de Toulouse, France, 1995).
7. B. Zappoli and A. Durand-Daubin, *Phys. Fluids* **6**:1929 (1994).
8. B. Zappoli, S. Amiroudine, P. Carlès, and J. Ouazzani, *J. Fluid Mech.* **316**:53 (1996).
9. P. Guenoun, D. Beysens, B. Khalil, Y. Garrabos, B. Kammoun, B. Le Neindre, and B. Zappoli, *Phys. Rev. E* **47**:1531 (1993).
10. M. Bonetti, F. Perrot, D. Beysens, and Y. Garrabos, *Phys. Rev. E* **49**:6 (1994).
11. D. Beysens, personal communication (1995).
12. S. Paolucci, *SAND* 82-8257 (1982).
13. S. V. Patankar, *Numerical Heat Transfer and Fluid Flow* (Hemisphere, Washington, DC, 1980).
14. B. P. Leonard and J. E. Drummond, *Int. J. Num. Methods Fluids* **20**:421 (1995).
15. T. Hayase, J. A. C. Humphrey, and R. Greif, *J. Comput. Phys.* **98**:108 (1992).